Optica Applicata, Vol. LII, No. 4, 2022
DOI: 10.37190/oa220404

Simultaneous intensity projection for projector response computation with application to an active radiometric calibration

Pedro-David FILIO-AGUILAR, Lourdes LÓPEZ-GARCÍA*,
Juvenal RUEDA-PAZ, Manuel ÁVILA-AOKI

CU-UAEM Valle de Chalco, Hermenegildo Galeana 3, Valle de Chalco,
Estado de México 56615, México

*Corresponding author: mllopezg@uaemex.mx

One of the most important sources of errors in digital fringe projection (DFP) systems is the nonlinearity in the response of the projector when it uses the three-step phase retrieval algorithm. Thus, it is necessary to increase the accuracy without affecting the efficiency. In this sense, the radiometric rectification methods are used. In this paper, an active radiometric rectification method for digital fringe projection is proposed. This proposal consists in two improvements of traditional active techniques: first, parallel intensity projection is used to obtain the projector response which requires only four dot patterns; and second, a method is provided for the calculation of the inverse polynomial that guarantees symmetry with respect to the response of the projector. Experimental results, in a digital fringe projection system, show that the root-mean-square phase error improves 6.3 times using this proposal.

Keywords: camera-projector compensation, digital fringe projection, phase retrieval, 3D imaging.

1. Introduction

The digital fringe projection (DFP) techniques have been widely used in areas such as entertainment, reverse engineering, and quality control, among others [1]. Commonly, this technique is based on the projection of sinusoidal fringe patterns using a digital projector and recorded with a digital camera. In this sense, the DFP techniques are affected by the nonlinearity of the input-to-output intensities of the projector whose goal is to enhance visual effects.

Several compensation methods have been proposed to eliminate such nonlinearity that can be grouped into two categories: active and passive methods. In the former, the sinusoidal fringe patterns are modified before their projection in such a way that the nonlinearity of the projector is cancelled [2]. In passive methods, the recorded fringe patterns are analyzed after their projection [3–8]. Active methods are faster than passive methods; they do not require any post-processing [9], however, it is assumed that the input-to-output response of the projector is previously known.

In practice, the projector response is obtained by projecting and recording uniform gray scale images with intensities from 0 to 255 onto a white dashboard. By analyzing a small window of each recorded image, the average of the intensities is taken as the output intensity. The previous process is time consuming and need to be performed if the projector and camera configuration are modified. Some authors have attempted to speed up the projector response acquisition by assuming an exponential model of the input-to-output response [10, 11]. Nevertheless, most common projector responses cannot be fitted using an exponential model.

In this research paper, we propose a method to speed up the projector response acquisition applied to an active compensation. This proposal is based on the projection of simultaneous dots with increasing gray level intensities. Four dot patterns containing 64 intensities each are projected to obtain several output intensities simultaneously. Latter, the obtained input-to-output response is used for an active compensation method in a DFP system. In addition, we propose a method for the calculation of the inverse polynomial. Experimental validation shows that the proposed method can obtain accurate projector responses compared to the traditional method.

The organization of this article is as follows: Section 2 discusses the principles of the DFP technique and the nonlinear response problem; Section 3 explains the proposed method for obtaining the input-to-output projector response and its application for an active compensation method; Section 4 presents the experimental validation, and Section 5 gives the conclusions.

2. Material and methods

2.1. The three-step phase retrieval algorithm

In phase shifting techniques, a sequence of discrete sinusoidal fringe patterns is projected over an object and the reflected intensities are imaged with a digital camera. The digitally generated fringe patterns are given by

$$I_k(i,j) = a\left[1 + \cos(2\pi j/p + \delta_k)\right] + b \tag{1}$$

where a is the amplitude intensity, p is the fringe pitch, δ_k is a known shift and b is the bias.

The recorded intensity images are described as

$$\tilde{I}_k(i,j) = I'(i,j) + I''(i,j)\cos\left[\varphi(i,j) + \delta_k\right] \tag{2}$$

where $I'(i,j)$ is the average intensity, $I''(i,j)$ is the intensity modulation, $\varphi(i,j)$ is the phase to be determined, and δ_k is the introduced shift.

The equation system given in Eq. (2) has three unknowns I', I'' and φ, which can be solved by a least squares approach for $k \geq 3$. For high-speed three-dimensional (3D) imaging, it is desirable to use the minimum number of fringe patterns. A particular solu-

tion for the three unknowns can be found when the measurements are taken at equally spaced intervals in a complete period. For instance, for $k = 3$ let $\delta_1 = -2\pi/3$, $\delta_2 = 0$ and $\delta_3 = 2\pi/3$, then the phase can be retrieved by

$$\varphi(i,j) = \tan^{-1}\frac{\sqrt{3}\,(\tilde{I}_1 - \tilde{I}_3)}{2\tilde{I}_2 - \tilde{I}_1 - \tilde{I}_3} \tag{3}$$

The retrieved phase given in Eq. (3) is known as the wrapped phase whose values range between $-\pi$ and π with a modulus of 2π. The process of removing the 2π discontinuities from the wrapped phase is called phase unwrapping [12]. Thus, the unwrapped phase together with the calibration data of the camera-projector system are used to obtain the 3D information through a phase-to-height method [13].

2.2. Active radiometric calibration

An active radiometric calibration method consists of pre-distort the sinusoidal fringe patterns before their projection, so as to compensate for the nonlinearity of the projector. HUANG *et al*. [2] and ZHANG [10] propose to model the projector response using a seventh order polynomial as

$$f(I_\mathrm{i}) = \sum_{k=0}^{7} a_k (I_\mathrm{i})^k \tag{4}$$

where I_i is the input intensity, $f(I_\mathrm{i})$ is the output intensity, and a_0, ..., a_7 are constants to be calibrated.

By determining the inverse polynomial f^{-1} it is possible to obtain the distorted fringe patterns as $I_k^{\mathrm{inv}} = f^{-1}(I_k)$. Thus, if the distorted patterns I_k^{inv} are projected, then the nonlinearity of the projector will be compensated.

For instance, Fig. 1(a) shows the ideal response, the actual projector response, the fitted polynomial model and its inverse polynomial model. Note that the initial and

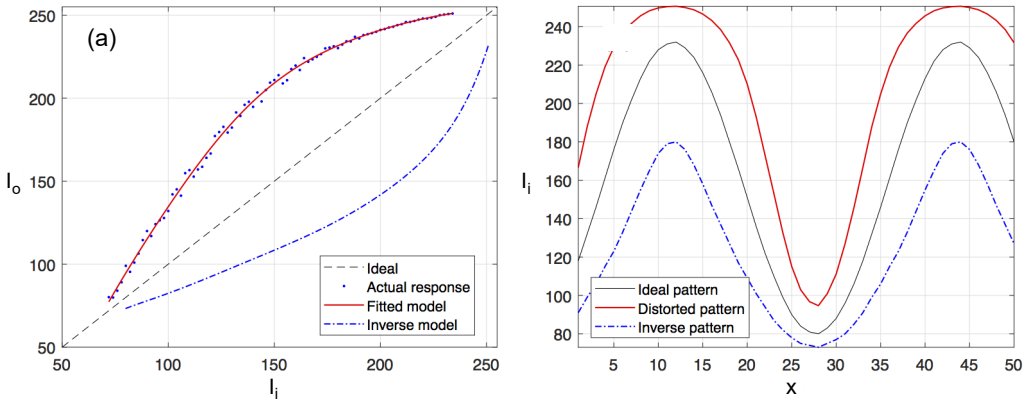

Fig. 1. Response of the projector (a). Ideal sinusoidal pattern and inverse sinusoidal pattern (b).

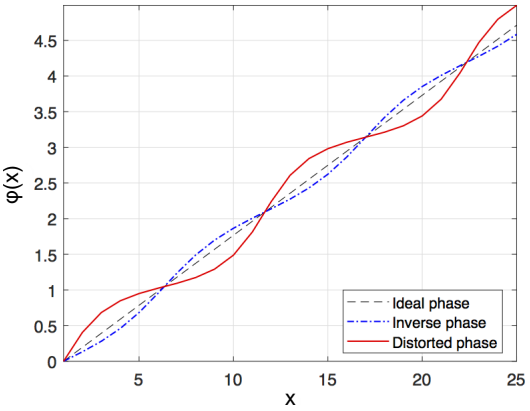

Fig. 2. Unwrapped retrieved phase using a three-step algorithm for ideal, distorted and inverse sinusoidal fringe patterns.

final intensity ranges were omitted in the projector response because the camera does not distinguish them. Figure 1(b) shows the ideal sinusoidal pattern as given in Eq. (1), the distorted sinusoidal pattern according to the polynomial model given in Eq. (4) and the pre-distorted sinusoidal pattern according to the corresponding inverse polynomial model. When the former inverse sinusoidal patterns are projected, the nonlinearity of the projector is canceled and thus almost ideal sinusoidal patterns is obtained. Finally, Fig. 2 shows the unwrapped retrieved phase using the three-step algorithm for ideal, distorted and inverse polynomial model. As can be seen, the nonlinearity of the projector affects severely the retrieved phase and thus introduces error in DFP systems.

3. Experimental method

This proposal for an active radiometric calibration method consists of two main steps. First, a strategy to speed up the computation of the camera-projector response by projecting in parallel several gray levels into four groups with increasing intensities is applied, and second, an improved computation of the inverse polynomial model is used and the error between the fitted polynomial model and the obtained inverse model is measured.

3.1. Parallel gray-levels projection

Commonly, the input-to-output response of a digital projector is obtained by projecting uniform gray-level images ranging from 0 to 255 over a white board and then taking the average intensity of a small window on the captured images. In other words, the response curve consist of a set of pairs $\{I_{i,k}, I_{o,k}\}$ for $k = 0, ..., 255$ where $\{I_{i,k}\}$ is the input gray scale to the projector and $\{I_{o,k}\}$ is the average intensity over the small window of the k-th captured image. This response curve of the camera-projector system

depends on the nonlinearities of the camera and projector, the angle of projection, and also on the local slope and the reflectivity of the measured object. Here, it is assumed that the configuration of the camera-projector and the measured object is static, and that the response of the camera is linear.

The above process is time-consuming and needs to be performed whenever the projector colour configuration changes. To speed up the acquisition of the input-to-output response, multiple regions are illuminated at the same time with continuous gray levels. Four dot patterns were designed with 64 continuous gray-levels each to cover the full range of 0 to 255. Each dot pattern contains 64 circles arranged as a lattice at the same distance from each other and with increasing intensity per row. It is assumed that each circle in the dot pattern affects a small and localized region of the scene from the point of view of the camera. The distance between the circles is such that the illuminated regions of each circle do not overlap with their neighbors.

Figure 3 shows a dot pattern with gray-level intensities from 192 to 255. The full range of 2^8 intensities was divided into four groups for two reasons: (1) to optimize the radius of the circles and the distance between them, and (2) to use the dot pattern with highest intensities for circles segmentation using global image thresholding by the method of Otsu [14]. To obtain the input-to-output response of the projector, first a correspondence was established between the projected circles and the segmented circles. Second, a histogram is constructed using the pixel intensities of each segmented circle, then it is averaged with the intensities of the highest frequency.

To cope with the influence of neighboring projected circles whose contributing intensities modify the true response curve the local regression smoothing to the projector response with parallel projection is used. This method allows to reduce the intensity variations introduced by projecting multiple gray-level intensities. The local regression smoothing helps to discard outlier intensities, large intensity variations in the obtained response curve, and overfitting. The MATLAB built-in smooth function within robust loss was used. Section 4 shows an example of the projector response obtained by parallel projection.

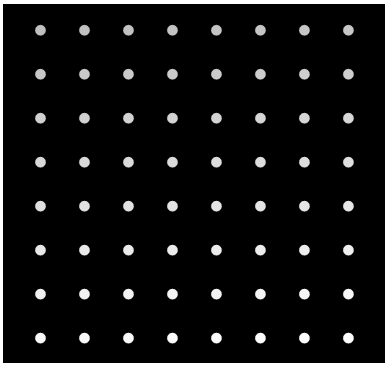

Fig. 3. Example of a dot pattern with intensities from 192 to 255.

3.2. Inverse polynomial computation

An important task in an active radiometric calibration method is the computation of the inverse polynomial. This problem cannot be solved for polynomials of degree greater than five. ZHANG [10] proposes to exchange the coordinates I_i and I_o of the actual response of the projector and then to fit a seventh order polynomial to the new data. However, this method does not guarantee that the fitted polynomial to the inverse data is symmetric with respect to the actual projector response.

Here, a variant of method of Zhang is proposed: (1) fit the seventh order polynomial to the actual projector response; (2) sample the polynomial on the range of interest; (3) exchange the coordinates of the sampled data and fit a second seventh order polynomial to the new data as follows:

$$f_{\text{inv}}(I_o) = \sum_{k=0}^{7} b_k (I_o)^k \tag{5}$$

This second polynomial given in Eq. (5) is used to generate the inverse sinusoidal fringe patterns as $I_k^{\text{inv}} = f_{\text{inv}}(I_k(j))$ for some $k \in \{1, 2, 3\}$ and $j = 1, ..., m$. To verify the accuracy of the generated inverse patterns, it defines the RMS error as

$$I_{\text{error}} = \sqrt{\frac{\sum_{j=1}^{m} \left[I_k(j) - f(I_k^{\text{inv}}(j)) \right]^2}{m}} \tag{6}$$

Thus, if the inverse fringe patterns were generated accurately, the error $I_{\text{error}} < \varepsilon$ for some positive threshold value ε. In practice, the value ε is not zero due to numerical inconsistencies in the computation of the inverse polynomial.

3.3. Proposed active radiometric calibration method

At this point, the proposed active radiometric calibration method can be summarized in the following steps:

1) Project and capture the intensities of the four groups of dots patterns as shown in Fig. 3, each one with sequential gray-levels from the intervals [0, 63], [64, 127], [128, 191], and [192, 255].

2) Obtain the projector response by parallel intensity projection as explained in Section 3.1.

3) Fit a seventh order polynomial on the data obtained in the previous step and determine its inverse polynomial as explained in Section 3.2.

4) Generate sinusoidal fringe patterns using inverse polynomial computed in the previous step.

5) Project the inverse sinusoidal fringe patterns (using the three-step phase retrieval algorithm) generated in the previous step and obtain the phase as given in Eq. (3).

In step 1), the full range of intensities from [0, 255] was splitted into four intervals, namely, [0, 63], [64, 127], [128, 191] and [192, 255]. For each interval [a, b], it is gen-

erated a dot pattern as shown in Fig. 3 with increasing intensities from *a* to *b*. The number of intervals and dots per pattern was chosen by experimentation such that minimize the number of projections. In step 2), the captured images are analyzed in order to detect each dot and its intensity, and thus obtain the response curve of the projector. In step 3), a seventh order polynomial to the obtained response curve of previous step is fitted, and the inverse polynomial is computed by interchanging the coordinates corresponding to the desired intensity and its captured intensity. Finally, in steps 4) and 5), the rectified fringe patterns are generated using the inverse polynomial, and then used to reconstruct the scene by fringe projection.

In Section 4 the proposed method to a DFP system for 3D imaging is applied.

4. Experiments and discussion

In this section, the experimental results obtained using the proposed active radiometric calibration method are shown. The infrastructure used in this research was the following: LG PW1000 DLP projector with a resolution of 1280 × 800 pixels; Canon EOS 1000D digital camera in RAW capture mode. The computational processing was performed on a laptop computer with an Intel Core i7-8750H CPU at 2.2 GHz, 16 GB of RAM, and the MATLAB software.

In Fig. 4(a) the projector configuration and the construction of the sinusoidal fringe patterns used to validation can be seen. It shows the projector response using parallel intensity projection and the fitted fourth order polynomial. A robust local regression with a span of 10% on the obtained projector response to alleviate the intensity variation was used. The dot patterns were generated using a radius of 20 pixels per circle with a distance of 98 pixels between them. The inverse sinusoidal fringe pattern can be seen in Fig. 4(b) together with the ideal and distorted patterns with a fringe pitch of 32 pixels.

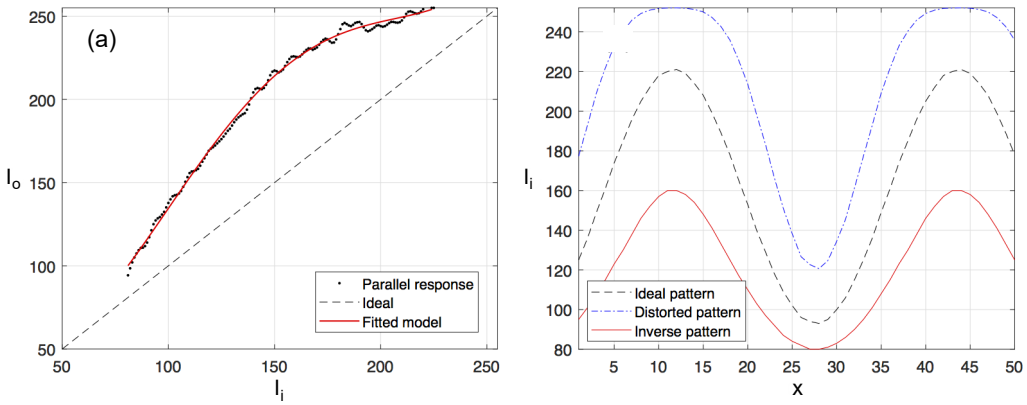

Fig. 4. Results using parallel projection: response curve and the fitted polynomial (a). Generated ideal, distorted and inverse sinusoidal fringe patterns (b). Square difference between ideal and modified inverse sinusoidal patterns (c).

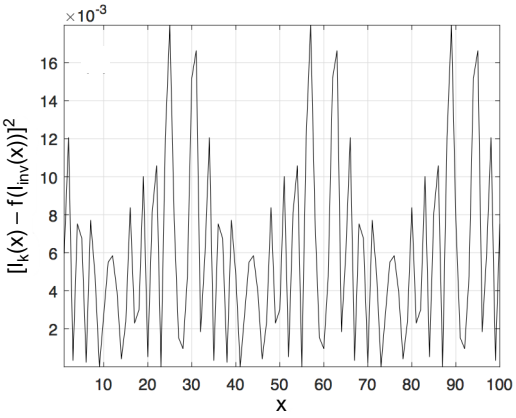

Fig. 4. Continued.

Notice that the intensities of the inverse and distorted sinusoidal patterns must be between the range of interest of the fitted polynomial. To ensure that this happens, we chose the amplitude $a = [f(\max(I_k)) - f_{\text{inv}}(\min(I_k))]/2$ and the bias value $b = f_{\text{inv}}(\min(I_k))$.

In Fig. 4(c), we can see the intensity square difference between the ideal I_k and modified inverse $f(I_k^{\text{inv}})$ patterns where f is the fitted polynomial. The resultant RMS error defined in Eq. (6) was $I_{\text{error}} = 0.00768$ pixels. The error I_{error} allows to measure the accuracy of the generated inverted fringe patterns, which may vary from thus obtained by the traditional method using the response curve shown in Fig. 1(a).

A comparison of the output intensity I_o obtained by projecting ideal and inverted fringe patterns on a flat surface is shown. The output intensity of ideal and inverted patterns can be seen in Fig. 5(a) and (b), respectively. The patterns were generated using a dynamic range between [93, 221] with parameters $a = 64$ and $b = 93$.

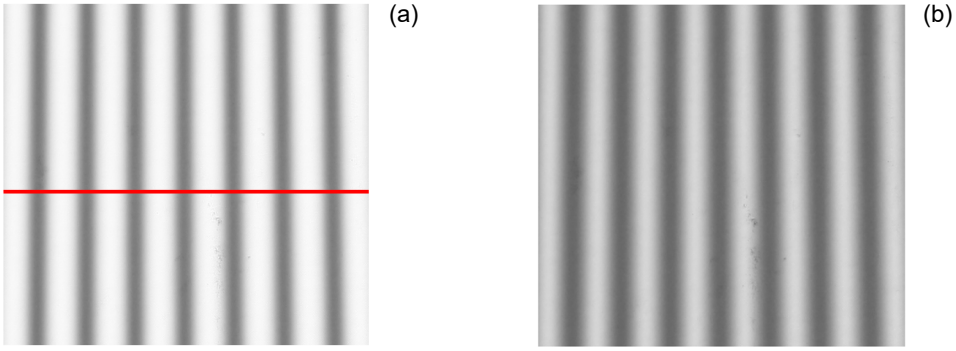

Fig. 5. Output intensity for ideal fringe patterns (a). Output intensity for inverted fringe patterns (b). Cross -section of the two patterns (c).

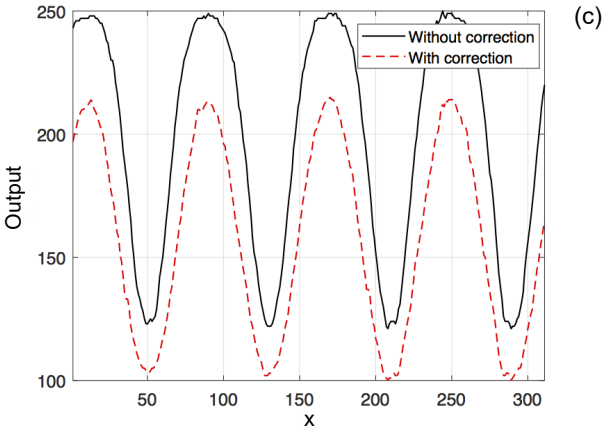

Fig. 5. Continued.

Figure 5(c) shows the horizontal cross-section marked in Fig. 5(a) for the two intensity patterns. Notice that the output intensity of the ideal patterns is out of dynamic range and the output intensity of the inverted patterns is within the established dynamic range.

4.1. Validation

The proposed method is validated by implementing a DFP system in two scenarios: a flat surface and an irregular object surface. The DFP system consists of the three-steps phase retrieval algorithm as shown in Section 2.1. Figure 6 shows the absolute phase of the flat surface obtained by projecting inverse patterns with the proposed method.

The 3D reconstruction of the flat surface with and without active radiometric correction can be seen in Fig. 7(a) and (b), respectively. The former shows that the waving

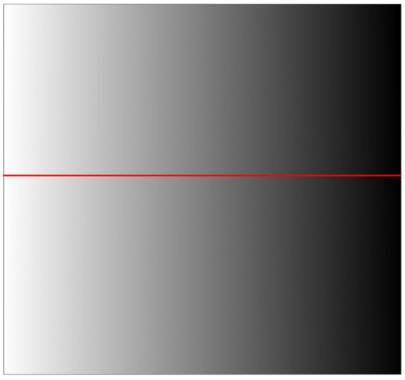

Fig. 6. 3D reconstruction results: absolute phase of the flat surface.

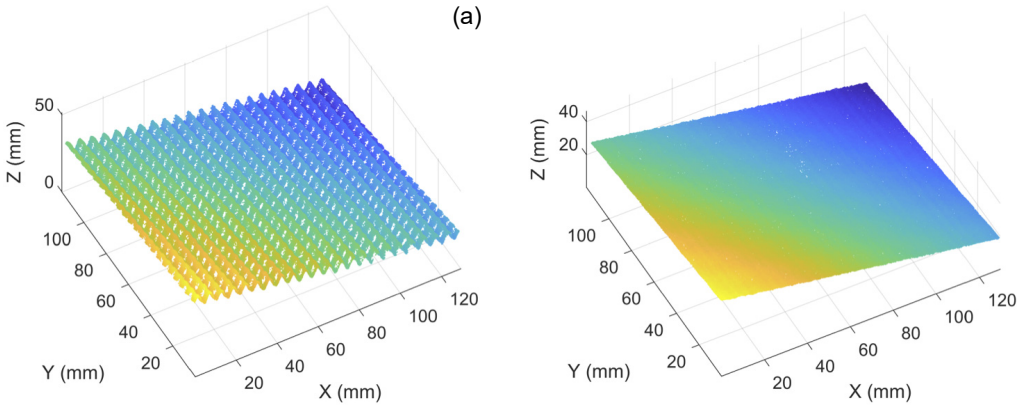

Fig. 7. Comparison of a 3D reconstruction of a flat surface: (a) without using radiometric correction, and (b) using the proposed active radiometric correction.

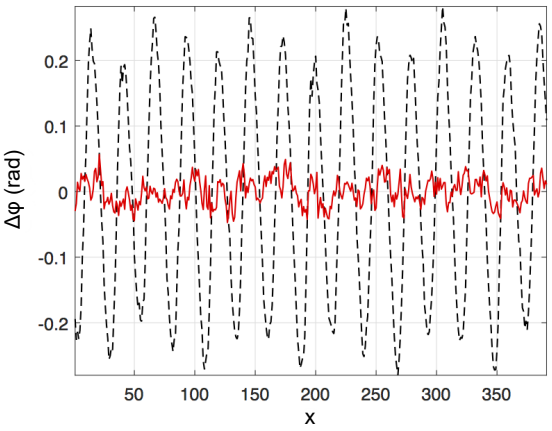

Fig. 8. Phase error comparison with and without radiometric correction; black dashed curve is the phase error without correction and red solid line is the phase error with correction.

structure of the surface is reduced drastically using our method in comparison to surface shown in Fig. 7(b) obtained without radiometric correction.

In addition, Fig. 8 shows the phase error through the red horizontal line, as shown in Fig. 6. Here, the phase error corresponds to the difference between a given phase line and an ideal phase line obtained through a 17-steps phase retrieval algorithm. The RMS error phase of the DFP system with and without radiometric correction were 0.0514 and 0.3276 rad, respectively. The proposed active radiometric method gives an improvement by factor of 6.3735 with a standard deviation of 0.0214 rad.

Figure 9(a) shows the results of the DFP system for the irregular surface in a picture of a white toy with a projected sinusoidal fringe pattern. Figure 9(b) shows a comparison of the absolute unwrapped phase for the horizontal red line marked in Fig. 9(a). As can be seen in Fig. 9(b), the phase without correction has a higher error compared

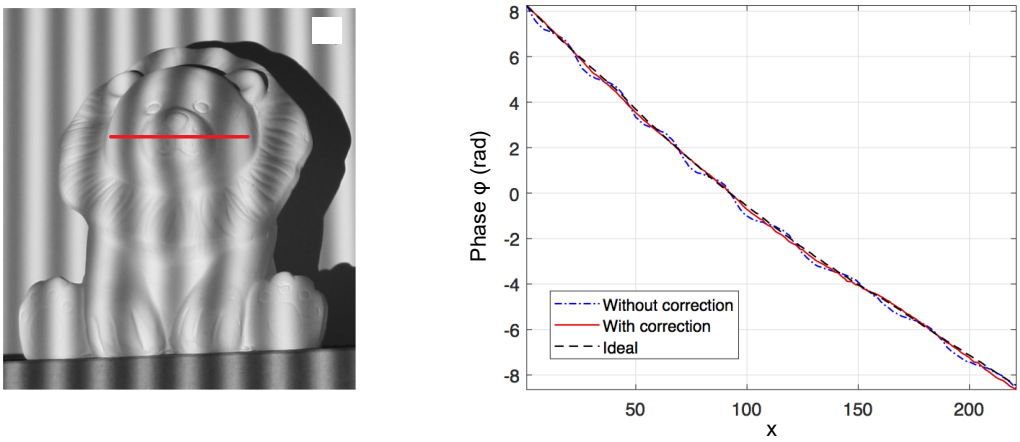

Fig. 9. 3D reconstruction results: a picture of an irregular surface (a). Comparison of the absolute unwrapped phases for the horizontal red line (b).

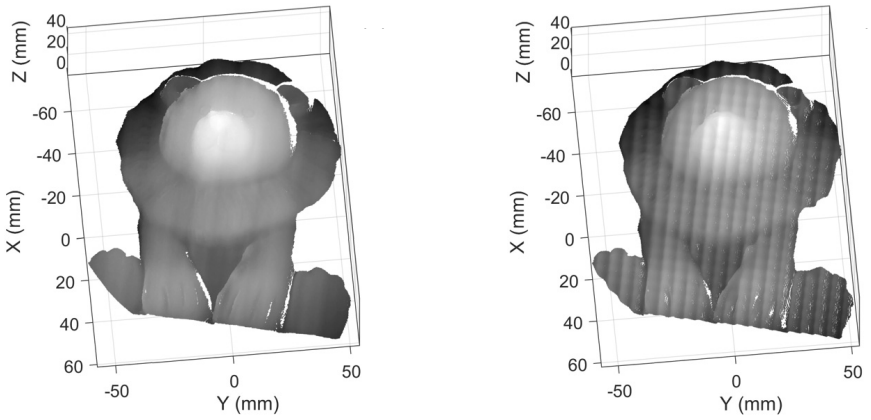

Fig. 10. 3D surface using the proposed method (a). 3D surface without radiometric correction (b).

with the ideal and corrected phases. Here, the ideal phase was obtained using a 17-steps phase retrieval algorithm. Figures 10(a), and (b) show the 3D surface with and without radiometric correction. In this scenario, the waving structure of the 3D surface reduces significantly with respect to the result without radiometric correction.

In the Table, we show a comparison of several methods for correcting the nonlinearity of the projector in DFP systems. To compare the different approaches, it shows the best phase error obtained under similar experimental conditions and scenarios. The phase error reported in [3] and [6] were 0.0651 and 0.0349 rad, respectively, both obtained by using an exponential model in order to determine the gamma parameter of the projector. In [4], a lookup table is constructed to store the phase error and used to compensate the obtained phase. The previous approach does not require obtaining the response curve of the projector, instead of that it projects sinusoidal fringe patterns us-

T a b l e. Comparison of different methods for correcting the nonlinearity of the projector.

Author	Method	Phase error [rad]
XIAO *et al*. [3]	Gamma model	0.0651
ZHANG and HUANG [4]	Phase compensation	0.01
ZHANG *et al.* [6]	Gamma model	0.0349
XING and GUO [8]	Harmonic analysis	0.0181
ZHANG [10]	Active correction	0.025
Our method	**Active correction**	**0.0514**

ing the three RGB color channels. A similar approach is reported in [8] in which a harmonic analysis is performed to compensate the phase. The phase error of methods [4] and [8] were 0.01 and 0.0181 rad, respectively. On the other hand, in [10], an active radiometric calibration method is used whose phase error was 0.025 rad and can be compared to the proposed method in this research which is 0.0514 rad. As can be seen, the accuracy of our method is near to the average phase error that is 0.03062 rad of the state of the art approaches presented in the Table.

4.2. Final remarks

An important limitation of active radiometric calibration methods is that the dynamic range is reduced. The latter is because the camera cannot distinguish the initial and final intensity intervals. In addition, to ensure that the intensity of inverse fringe patterns is within the established dynamic range, it is necessary to further reduce the dynamic range. Some authors have tried to extend the dynamic range by changing the camera exposure [15] and by generating inverse and regular fringe patterns depending on the saturated imaged patterns [16]. Thus, it is of interest to study the relationship between the nonlinearity of the project and high dynamic range (HDR) techniques.

Although the parallel intensity projection speeds up the exhaustive projection of gray levels, it has some restrictions that have to be taken into account: (1) it requires a large whiteboard to project the dot patterns, and (2) the distance between the dots should be as large as possible to avoid overlapping the illuminated areas. Other kinds of patterns can be designed in order to alleviate these restrictions, for instance, by generating colours pattern [11].

5. Conclusions

An active radiometric calibration method has been proposed whose accuracy is similar to the state of the art techniques. A parallel intensity projection was used to obtain the projector response using only four dot patterns which speed up exhaustive projection of 256 gray-levels. Also, a method to compute the inverse polynomial used to generate the inverse sinusoidal fringe patterns was proposed. This last method allows us to ensure that the inverse polynomial is symmetric with respect to the fitted polynomial on the approximated projector response. Finally, it is validated that the proposal can

improve the RMS phase error by 6.3735 times in a DFP system without radiometric calibration.

Acknowledgements
This work was supported by the CONACyT Scholarship number 481858.

References

[1] Zuo C., Feng S., Huang L., Tao T., Yin W., Chen Q., *Phase shifting algorithms for fringe projection profilometry: A review*, Optics and Lasers in Engineering **109**(2), 2018, pp. 23–59, DOI: 10.1016/j.optlaseng.2018.04.019.

[2] Huang P.S., Zhang C., Chiang F.P., *High-speed 3-D shape measurement based on digital fringe projection*, Optical Engineering **42**(1), 2003, pp. 163–168, DOI: 10.1117/1.1525272.

[3] Xiao Y., Cao Y., Wu Y., Shi S., *Single orthogonal sinusoidal grating for gamma correction in digital projection phase measuring profilometry*, Optical Engineering **52**(5) 2013, article no. 053605, DOI: 10.1117/1.OE.52.5.053605.

[4] Zhang S., Huang P.S., *Phase error compensation for a 3-D shape measurement system based on the phase-shifting method*, Optical Engineering **46**(6), 2007, article no. 063601, DOI: 10.1117/1.2746814.

[5] Liu K., Wang Y., Lau D.L., Hao Q., Hassebrook L.G., *Gamma model and its analysis for phase measuring profilometry*, Journal of the Optical Society of America A **27**(3), 2010, pp. 553–562, DOI: 10.1364/JOSAA.27.000553.

[6] Zhang X., Zhu L., Li Y., Tu D., *Generic nonsinusoidal fringe model and gamma calibration in phase measuring profilometry*, Journal of the Optical Society of America A **29**(6), 2012, pp. 1047–1058, DOI: 10.1364/JOSAA.29.001047.

[7] Li B., Wang Y., Dai J., Lohry W., Zhang S., *Some recent advances on superfast 3D shape measurement with digital binary defocusing techniques*, Optics and Lasers in Engineering **54**, 2014, pp. 236–246, DOI: 10.1016/j.optlaseng.2013.07.010.

[8] Xing S., Guo H., *Correction of projector nonlinearity in multi-frequency phase-shifting fringe projection profilometry*, Optics Express **26**(13), 2018, pp. 16277–16291, DOI: 10.1364/OE.26.016277.

[9] Lü F., Xing S., Guo H., *Self-correction of projector nonlinearity in phase-shifting fringe projection profilometry*, Applied Optics **56**(25), 2017, pp. 7204–7216, DOI: 10.1364/AO.56.007204.

[10] Zhang S., *Comparative study on passive and active projector nonlinear gamma calibration*, Applied Optics **54**(13), 2015, pp. 3834–3841, DOI: 10.1364/AO.54.003834.

[11] Shahpaski M., Ricardo Sapaico L., Chevassus G., Susstrunk S., *Simultaneous geometric and radiometric calibration of a projector-camera pair*, [In] *2017 IEEE Conference on Computer Vision and Pattern Recognition* (*CVPR*), IEEE, 2017, pp. 3596–3604, DOI: 10.1109/CVPR.2017.383.

[12] Ghiglia D.C., Pritt M.D., *Two-Dimensional Phase Unwrapping: Theory, Algorithms, and Software*, Wiley-Interscience, Chapter 1. pp. 1–30.

[13] Lu J., Mo R., Sun H., Chang Z., *Flexible calibration of phase-to-height conversion in fringe projection profilometry*, Applied Optics **55**(23), 2016, pp. 6381–6388, DOI: 10.1364/AO.55.006381.

[14] Otsu N., *A threshold selection method from gray-level histograms*, IEEE Transactions on Systems, Man, and Cybernetics **9**(1), 1979, pp. 62–66, DOI: 10.1109/TSMC.1979.4310076.

[15] Zhao H., Liang X., Diao X., Jiang H., *Rapid in-situ 3D measurement of shiny object based on fast and high dynamic range digital fringe projector*, Optics and Lasers in Engineering **54**, 2014, pp. 170–174, DOI: 10.1016/j.optlaseng.2013.08.002.

[16] Jiang C., Bell T., Zhang S., *High dynamic range real-time 3D shape measurement*, Optics Express **24**(7), 2016, pp. 7337–7346, DOI: 10.1364/OE.24.007337.

Received September 16, 2021
in revised form December 11, 2021